# *Final Draft*
**of the original manuscript:**

Cardillo, M.E.B.; Shen, J.; de Alcantara, N.G.; Afonso, C.R.M.;
dos Santos, J.F.:

**Effect of friction spot welding parameters on the joint formation and mechanical properties of Al to Cu**

In: Welding in the World (2018) Springer

DOI: 10.1007/s40194-018-0632-4

# Effect of friction spot welding parameters on the joint formation and mechanical properties of Al to Cu

Maria E. B. Cardillo[a], Junjun Shen[b*], Nelson G. de Alcântara[a], Conrado R. M. Afonso[a], Jorge F. dos Santos[b]
[a] Federal University of Sao Carlos (UFSCar), Department of Materials Engineering (DEMa), Rodovia Washington Luiz – km 235, 13565-905 Sao Carlos, SP, Brazil
[b] Helmholtz-Zentrum Geesthacht GmbH, Institute of Materials Research, Materials Mechanics, Solid State Joining Processes (WMP), Max-Planck-St. 1, D-21502 Geesthacht, Germany
*Corresponding author. E-mail: junjun.shen@hzg.de

**Abstract**

Friction spot welding is an appealing technique for joining dissimilar materials, such as aluminum and copper that have significant differences in physical and mechanical properties. To optimize the welding process, a full-factorial design was employed. It is found that in addition to the plunge depth, the interaction between the rotational speed and the plunge depth significantly influences the lap-shear strength of the Al/Cu dissimilar joints. Further investigations on macro- and microstructures show that increasing the plunge depth could deform the Cu sheet into a concave shape to form a mechanical interlocking, and thus increases the joint lap-shear strength; increasing the tool rotational speed, however, may compromise this effect because of the formed tunnel defects on the interface due to high thermal exposure.

Keywords: friction spot welding (refill friction stir spot welding); dissimilar; aluminum; copper; microstructures; mechanical properties

## 1 Introduction

The Al/Cu dissimilar joint has been widely applied in industries for its mass and cost reduction [1, 2]. The welding technique is, however, still in challenging and impeding its applications. Traditional fusion welding methods are rarely used because of the compromised mechanical properties caused by the formed brittle intermetallic compounds. [3, 4] Therefore, more reliable welding techniques are required.

Friction spot welding (FSpW) is a solid-state joining technique developed and patented by Helmholtz-Zentrum Geesthacht (HZG, formerly known as GKSS Forschungszentrum Geesthacht) in 1999. [5] Figure 1 shows the principle of the process via the sleeve-plunge variant. At the beginning, the clamping ring holds the materials against the backing (Figure 1a). Then, the sleeve rotates and plunges downward into the material, meanwhile the rotating pin moves upward synchronously (Figure 1b). At this stage, a softened plasticized-material rod and a local softened keyhole are formed by the frictional heating and plastic deformation. If necessary, this stage can be facilitated by holding the sleeve at the desired

depth (Figure 1c). Finally, the sleeve and the pin return to their original position, forging the softened rod back into the keyhole, resulting in a keyhole-free joint (Figure 1d).

Because of its solid-state characteristic and advantages such as the superior resultant mechanical properties and the keyhole-free joint surface finish [6, 7], FSpW can be an alternative process to replace resistance spot welding (RSW) or friction stir spot welding (FSSW) for welding similar materials. More importantly, in FSpW, the sleeve or pin does not necessarily penetrate thoroughly through the upper sheet [8, 9], and thus the hook, which is inevitable and undesirable in FSSW, can be avoided. This makes it advantageous over FSSW in welding dissimilar materials. In our previous studies [10, 11], the good friction spot weldability for Al/Cu dissimilar joints and a eutectic liquefaction due to a relatively high temperature and mass transport of Cu have been demonstrated. So far, no systematic investigation has been undertaken for Al/Cu joints that correlates the process parameters with the mechanical properties and macro/microstructures.

Design of experiments (DOE) technique is a powerful methodology often used in industrial experimentation for exploring the effects of process variables on the product quality. [12] The objective of this research is to determine the optimal parameter settings via DOE, and investigate the influence of welding parameters on the joint microstructure and mechanical property.

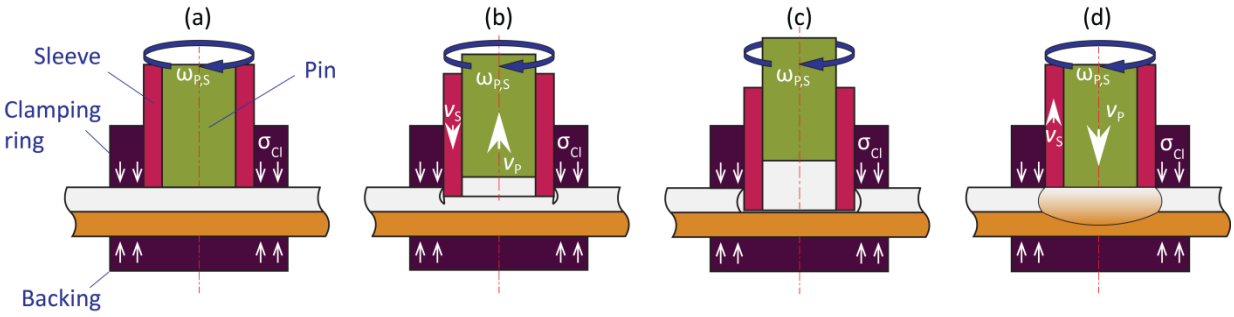


Figure 1. Schematic representation of the FSpW process−sleeve-plunge variant: (a) loading; (b) plunging; (c) dwelling; and (d) retracting. ($\sigma_{cl}$: clamping force, $\omega_{P,S}$: rotational speed of the pin and the sleeve, $v_{P,S}$: the linear velocity of the pin and the sleeve)

## 2 Experimental materials and procedure

### 2.1 Base metal and experimental procedure

The base metals used were commercially available AA5083 Al alloy (referred to as Al) and phosphorus deoxidized copper sheets (the chemical composition and mechanical properties shown in Table 1) with dimensions of 100 ×25 ×2 $mm^3$. The overlap spot welds, the Al sheet being placed on top of the copper (referred to as Cu) sheet, were produced using an RPS 100 machine and a threaded tool

with diameters of 14.5, 9, and 6 mm for the clamping ring, sleeve, and pin, respectively. During welding, the temperature of the weld center was measured by a K-type thermocouple embedded at the initial Al/Cu interface and recorded with a frequency of 50 Hz.

After welding, the samples for metallurgical observation were first cut by using a wheel cutting machine, and subsequently ground and polished according to the standard metallurgical program. Following that, the samples were etched by Dix-Keller etchant (a solution of 190 ml $H_2O$, 5 ml $HNO_3$, 3 ml HCl, and 2 ml HF) for 45 s at the room temperature to reveal the macro/micro features by an optical microscope (OM). Followed by being polished on a cross section polisher, those representative specimens were analysed by a scanning electron microscope (SEM) equipped with an energy dispersive spectrometer (EDS) and an electron backscatter diffraction (EBSD) system.

The lap-shear strength (LSS) was chosen to evaluate the weld quality since this property is of interest and a good indicator to the weld mechanical properties. The lap-shear test was carried out on a universal testing machine, Zwick/Roell 1478, at a constant crosshead speed of 1 mm/min. To produce statistical significance to the results, three repetitions were tested for each welding condition. After lap-shear tests, the fracture surfaces were analyzed by using SEM and a digital camera.

Table 1 Nominal chemical composition and mechanical properties of Cu-DHP and AA 5083

| Material | Chemical composition (wt. %) | | | | | | | | | Mechanical properties | |
|---|---|---|---|---|---|---|---|---|---|---|---|
| | Al | Cr | Cu(Ag) | Fe | Mg | Mn | P | Si | Zn | $\sigma_b$ (MPa) | δ (%) |
| Cu-DHP | — | — | >99.9 | — | — | — | 0.015-0.04 | — | — | 274 | 26 |
| AA5083 | Bal. | <=0.25 | <=0.1 | <=0.4 | 4.0-4.9 | 0.4-1.0 | — | <=0.4 | <=0.25 | 290 | 25 |

### 2.2 Design of experiments

The effect of FSpW process parameters on the mechanical performance of the joints was analyzed by using DOE via a Taguchi $L_9$ orthogonal array at first. According to the percent contribution (calculation method see [13]) by analysis of variance (ANOVA), the sleeve plunge depth (hereafter referred to as plunge depth) contributes most to joint LSS, however, slightly higher than the experimental residual error does. This implies that the interactions between the main factors, having not been included, probably contribute large. To consider the interactions, a follow-up two-level full-factorial design of experiments ($2^3$) was carried out by using the same factors at the levels shown in Table 2. Minitab [14] software was used for assisting the analysis of experimental results.

Table 2 Factors and levels studied in the experiment for full-factorial design

| Factors | Designation | Levels | |
|---|---|---|---|
| | | 1 | 2 |
| Tool rotational speed (rpm) | *R* | 1200 | 2000 |
| Sleeve plunge depth (mm) | *D* | 1.8 | 2.0 |
| Dwell time (s) | *T* | 1 | 2 |

## 3 Results and discussions

### 3.1 Full-factorial design

Table 3 presents the full-factorial design and the LSS as the response for each condition. Data normality assumption is verified via the NPP (Normal Probability Plot) of residuals, which is not shown here.

Table 3. Experimental results for average using a full-factorial design of $L_8$ ($2^3$)

| Trial | *R* (rpm) | *D* (mm) | *T* (s) | Average LSS (kN) |
|---|---|---|---|---|
| 1 | 1200 | 1.8 | 1 | 3.51 |
| 2 | 1200 | 2 | 2 | 7.10 |
| 3 | 2000 | 2 | 1 | 6.68 |
| 4 | 1200 | 2 | 1 | 6.72 |
| 5 | 1200 | 1.8 | 2 | 4.37 |
| 6 | 2000 | 1.8 | 1 | 4.59 |
| 7 | 2000 | 1.8 | 2 | 4.99 |
| 8 | 2000 | 2 | 2 | 5.32 |

(1) Interactions

The Pareto plot allows detecting the main and interaction effects that are most important to the process [12]. It displays the absolute value of the effects and draws a reference line on the chart. Any effect that extends beyond this reference line is potentially important. The Pareto plot for the designed model is given in Figure 2, where the dashed red line denotes the reference *t* ($t_{n,\ 1-\alpha/2}$= $t_{3,\ 0.975}$= 3.182, the (1-α/2) quantile of a *t*-distribution with DOF equal to that for the error term). Obviously, factor *D* and interaction *R*×*D* are most important. This can also be confirmed by the main effects plot, as shown in Figure 3, that factor *R* (the tool rotational speed, hereafter referred to as rotational speed) and factor *T* (the dwell time) have a much lower sensitivity to variability in LSS in comparison with the plunge depth (factor *D*). In the meantime, Figure 4 clearly indicates the existence of interaction between factors *R* and *D*; the effects of plunge depth (factor *D*) at different levels of rotational speed (factor *R*) are different.

(2) Analysis of variance

Table 4 shows the results of ANOVA. It suggests, in addition to that for factor *D*, the calculated value of variance ratio *F* for interaction *R*×*D* is also greater than the critical *F* value (10.128) within the

confidence level. This means that the influence of rotational speed on the LSS is significantly dependent on the plunge depths, which is also confirmed by the *p*-test, *i.e.*, the *p*-values of factor *D* and interaction *R*×*D* are below α= 0.05. That is, except for factor *D*, interaction *R*×*D* also contributes evidently to the response at 95% confidence level. In this sense, the low level (1200 rpm) should be selected for factor *R* to enhance the LSS of the joints.

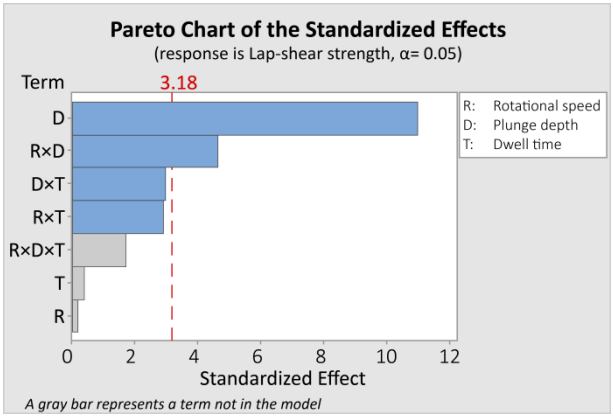


Figure 2: Pareto plot analysis of the main effects and interactions

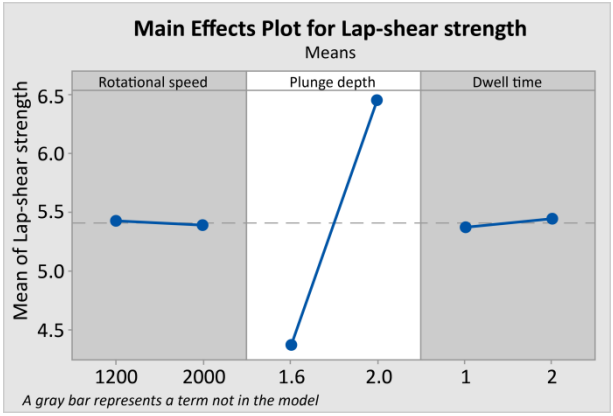


Figure 3. Effect of each level on the mean of LSS: (a) rotational speed, (b) plunge depth, and (c) dwell time. (factors *R* and *T* are pooled)

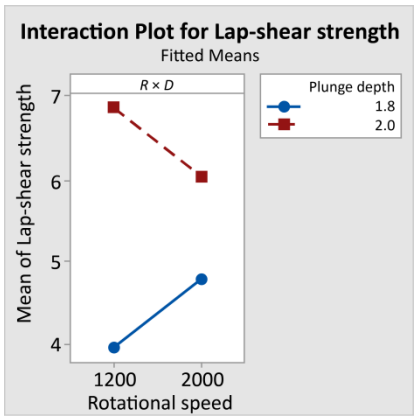


Figure 4. Interaction plot for LSS: *R*×*D*

Table 4. Analysis of variance table for the average

| Source | DOF | Sum of squares | Variance | *F* | S' | *p* | *P*% |
|---|---|---|---|---|---|---|---|
| *R* | (1) | (0.0018) | *Pooled* | | | | |
| *D* | 1 | 8.74 | 8.74 | 121.11 | 8.66 | 0.002 | 73.84 |
| *T* | (1) | (0.0098) | *Pooled* | | | | |
| *R*×*D* | 1 | 1.55 | 1.55 | 21.47 | 1.48 | 0.019 | 12.58 |
| *R*×*T* | 1 | 0.61 | 0.61 | 8.39 | 0.53 | 0.063 | 4.54 |
| *D*×*T* | 1 | 0.63 | 0.63 | 8.70 | 0.56 | 0.06 | 4.73 |
| *R*×*D*×*T* | (1) | (0.20) | *Pooled* | | | | |
| Error | 3 | 0.22 | 0.07 | 1 | 0.50 | | 4.30 |
| Total | 7 | 11.73 | | | | | 100 |

$F_{.05}(1, 3) = 10.128$

In summary, the results above indicate that the optimal setting for maximizing the LSS is 1200 rpm for rotational speed, 2 mm for plunge depth, and 2 s for dwell time. The mean maximum LSS is 7.1 kN. It is much higher than the minimum average load of 4.76 kN that is recommended for resistance spot welded aluminum alloys of the same thickness [15]. This demonstrates that dissimilar friction spot welded joints can yield good mechanical properties.

### 3.2 Representative fracture modes

Figure 5 shows two representative fracture surfaces of joints and their corresponding cross-sections. Unlike in RSW where joints usually fracture by means of interfacial failure or nugget pullout, the joints produced by FSpW in this research fail only along the interface. According to the shape of the interface, the failure can take place in two modes, Mode I and Mode II, as shown in Figures 5a and 5c. The difference is that in Mode I little plastic deformation takes place prior to fracture, and in Mode II more deformation was involved. Thus, Mode II is associated with higher load-bearing capacity than Mode I. This can also be manifested by the corresponding displacement–load curves, as shown in Figure 6. The fracture energy (calculated from the area below the displacement–load curve) of a joint failed by Mode II (dark cyan curve) is more than 5 times of that of a joint failed by Mode I (gray curve). It is noted that these two curves have nearly the same slope starting from a certain stage, which means that the load-bearing parts have the same Young's Modulus, that is, the load-bearing structures have the same components (microstructure). However, the dark cyan curve is obviously above the gray one. This is most likely because of the mechanical interlocking effect in Mode II due to the depressed Cu sheet (Figure 5c). For the same reason, as increasing the displacement, the crack propagation is restrained by the interlock in Mode II, and thus the loading could keep increasing while the flat interface fails shortly in Mode I. Moreover, it seems that the weld center (indicated by the inner black circle in Figure 5) has little

contribution to the weld's strength no matter of the interface morphology, which means that the Al/Cu interface around the weld center has a low fracture toughness.

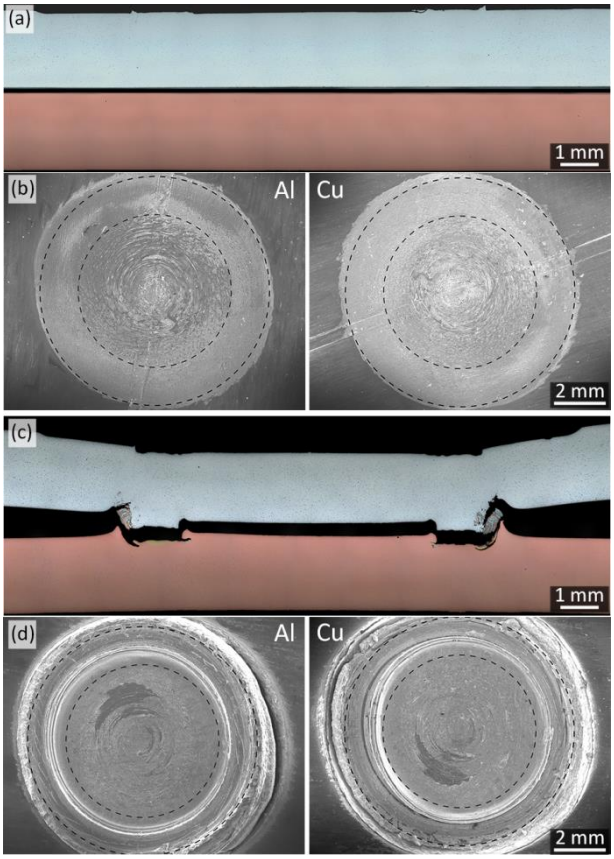


Figure 5. Representative fracture modes: Mode I (a) cross-sectional view (OM), (b) top view (SE) and mode II (c) cross-sectional view (OM), (d) top view (SE) (dashed black lines demote the contour lines of the pin and the sleeve)

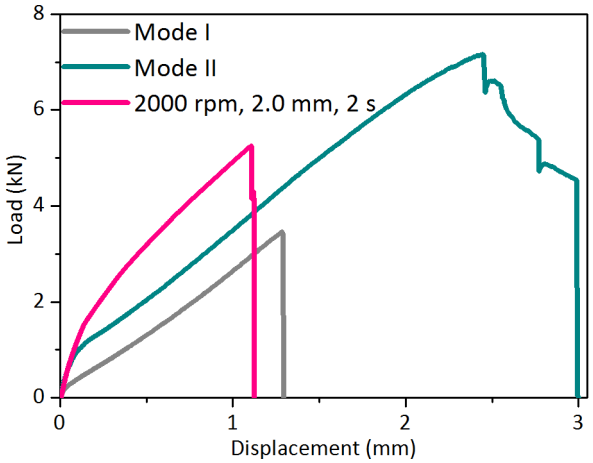


Figure 6. Representative load–displacement curves obtained from the lap-shear test

### 3.3 Influence of welding parameters on joint macro- / microstructures and fracture modes

(1) Representative microstructures

The representative microstructures developed in Al/Cu welds produced by FSpW have been separately described in previous studies [10, 11], which are summersied in Figure 7. In general, the weld

nugget is symmetrically drum-shaped without visible hook or cracking. The rim of the weld nugget (the border of the stir zone) shows a completely different contrast. The Al/Cu interface, however, is of more interest as the primary fracture path under tension loading. At a mild condition, the Al/Cu interface shows flat features (Figure 7a), surrounded by plenty of fine particles (Figures 7b and 7c), i.e., $MgCuAl_2$ and $Al_6(Mn, Fe)$, according to the integrated EDS and EBSD result (not shown here). As common in Al/Cu friction stirred welds, the interface consists of a $CuAl_2$-$Al_4Cu_9$ composite layer [16, 17] of varied thickness, *e.g.*, less than 0.2-0.3 μm under the sleeve (Figure 7b) and 0.5-1.2 μm at the center (Figure 7c). At a harsh condition, the Al/Cu interface shows more deformed features (Figure 7d), alongside with regions of dark contrast, which may be the product of local eutectic liquefaction (Al-$MgCuAl_2$ eutectic) that is associated with the mass transport induced by material flow and severe plastic deformation [10]. However, the interface consists of the same composite layer but slightly thicker (Figures 7e and 7f).

Certainly, these macro- and microstructures, as the result of the thermo-mechanical process, are correlated with the welding parameters. As previously mentioned in part 3.1, the rotational speed and dwell time are insignificant to the joint LSS, therefore, only the influence of the plunge depth and the interaction between rotational speed and plunge depth will be considered.

(2) The influence of the plunge depth

Figure 8 shows the joints produced under different plunge depths ($R$= 1200 rpm, $T$= 2 s) and the corresponding fracture surfaces after the lap-shear test. As increasing the plunge depth, the weld rim becomes larger and deeper, as shown in Figures 8a and 8b. Further increasing the plunge depth, *e.g.*, 2.0 mm, the lower copper sheet will be also evidently depressed by the severe plastic deformation due to the approaching of the sleeve, and thus a cave is formed on the Al/Cu interface right beneath the sleeve end face. At the micro level, however, the influence of the plunge depth on the formation of intermetallic composite layer is limited, similar to what was shown in Figure 7. In fact, the peak temperature of the Al/Cu interface obtained under different plunge depths does not change markedly (*see* Table 5), which implies that the Al/Cu interfacial structures are nearly unchanged with increased plunge depth. Nevertheless, as discussed in part 3.2, it is most likely the cave rather than the microstructure that changes the propagation path of cracking (see also Figure 8) and the failure mode, and thus significantly increases the LSS. On the contrary, an increase in rotational speed or dwell time could also enlarge the weld rim, however, hardly increase the depth of the weld nugget or form a cave on the bottom sheet. Therefore, the effects of the rotational speed and the dwell time are statistically insignificant to the LSS of the joints.

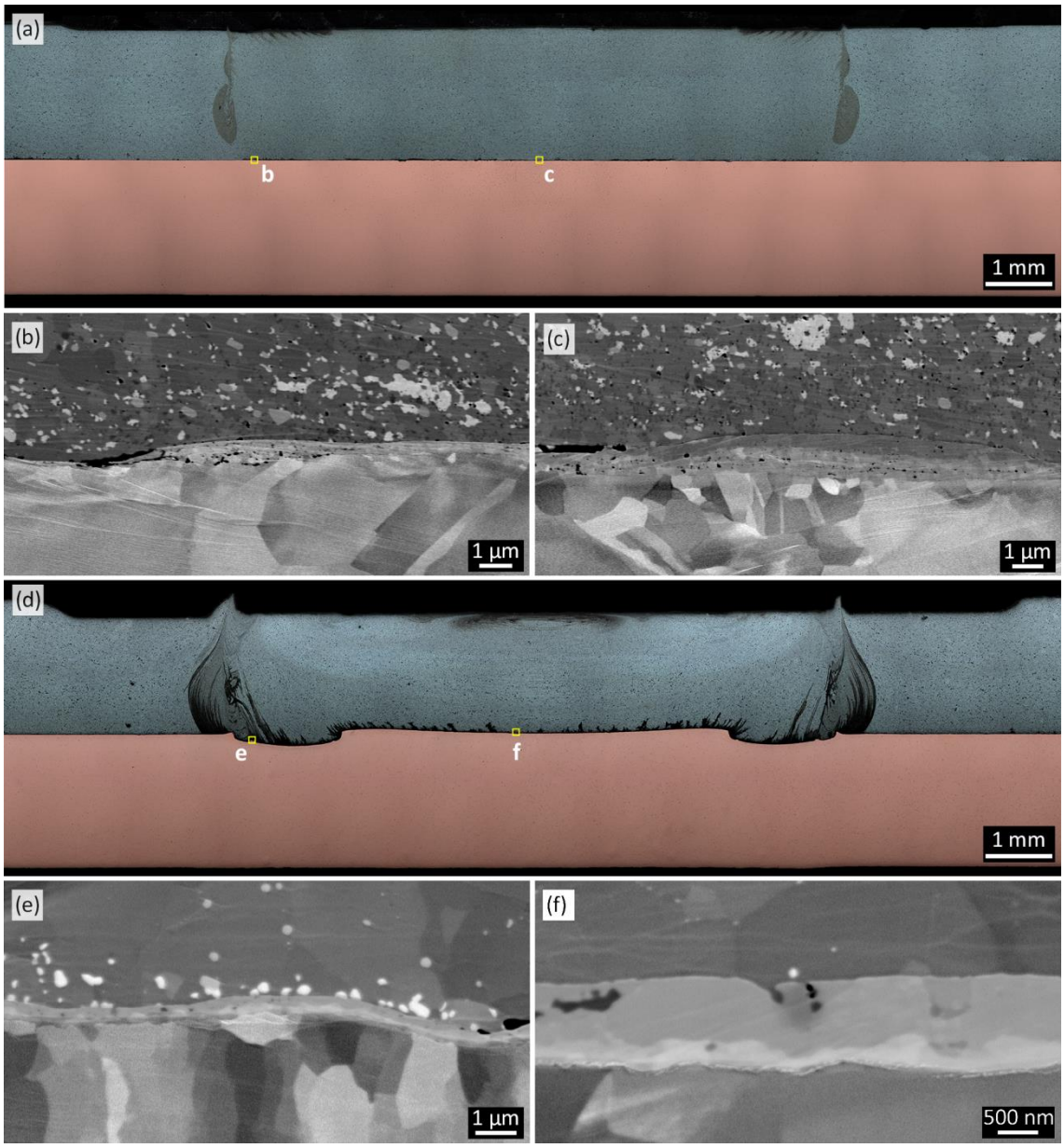


Figure 7. Representative macro- and microstructure of joints produced under different welding parameters: *R*= 1200 rpm, *d*= 1.6 mm, *T*= 0 (a) overview and (b) (c) magnified view of locations b, c; *R*= 2000 rpm, *d*= 2 mm, *T*= 1 s (d) overview and (e) (f) magnified view of locations e, f. (Rectangles b, c, e, and f show the locations of selected areas)

(3) The influence of the interaction R×D

To demonstrate the effect of the interactions of rotational speed and plunge depth, another two joints produced under different plunge depths (*R*= 2000 rpm, *T*= 2 s) are shown in Figure 9 in comparison with Figures 8b and 8c. As mentioned above, a large plunge depth could cause the copper sheet to depress to form a cave and facilitate the mechanical interlocking effect that changes the fracture mode. However, at a large plunge depth, the joint of *R*= 2000 rpm shows a much smoother fracture surface (Figures 8c and 9b) in comparison with that of *R*= 1200 rpm. Also, in the load-displacement curve (Figure 6), the one obtained from the joint produced under *R*= 2000 rpm, *T*= 2 s, *d*= 2 mm (in pink) suddenly failed prior to

obvious deformation, although it has an evidently large slope at the beginning. This can be most likely attributed to the cavity defect formed at the Al/Cu interface, as shown in Figure 10. This defect may be more precisely named tunnel defect that most likely runs circumferentially, since a similar cavity was also formed at the same location on the other side of the weld.

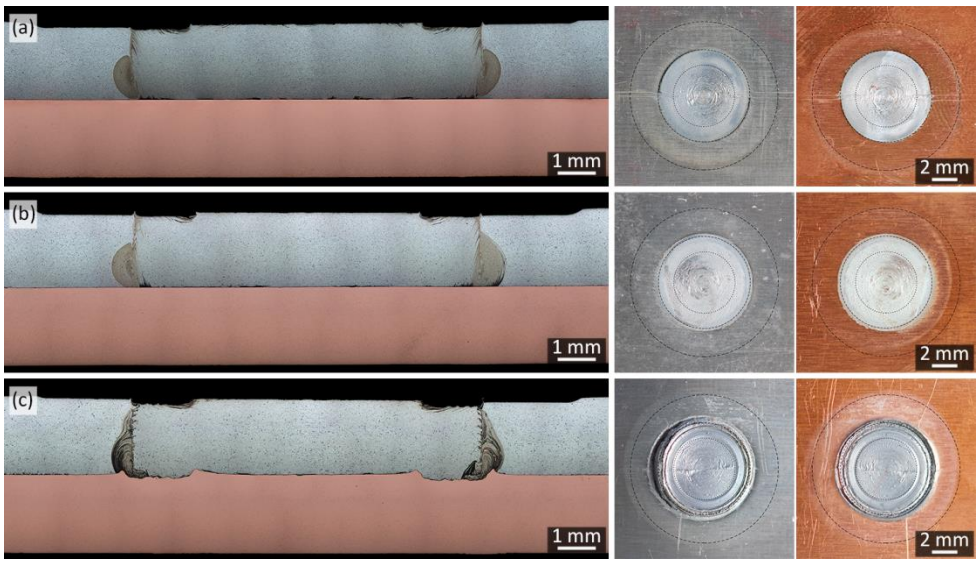


Figure 8. Joints produced under different plunge depths and the corresponding fracture surfaces, *d*= (a) 1.6 mm (b) 1.8 mm (c) 2.0 mm (*R*= 1200 rpm, *T*= 2 s)

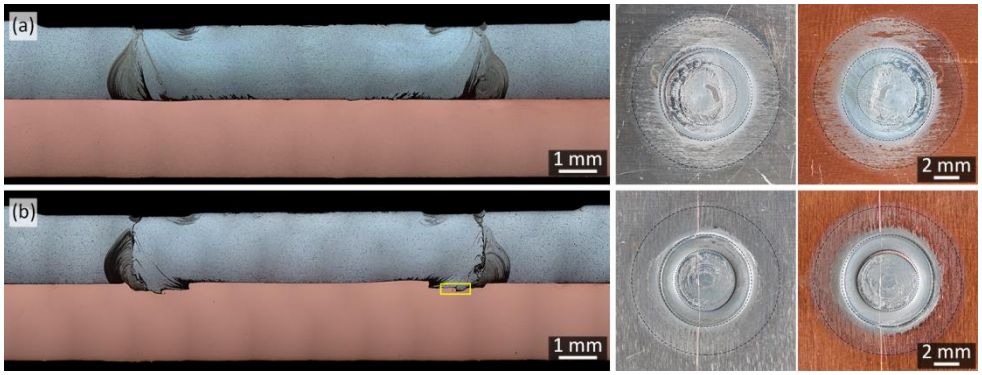


Figure 9 Comparison with the result of Figure 8 in relation to the interaction of the plunge depth and the rotational speed, *d*= (a) 1.8 mm (b) 2 mm (*R*= 2000 rpm, *T*= 2 s)

This kind of tunnel defect has not been found in joints under other welding parameters or in literature of FSpW. It may be interpreted as follows. On one side, when the rotational speed is high, the peak temperature of the weld can reach or even exceed the melting point of certain eutectic reactions, such as Liquid⇌(Al)+ $MgCuAl_2$. In a previous study [10], the ternary eutectic structures Al-$MgCuAl_2$ were observed ~100 μm away from the Al/Cu interface. Compared to that sample, the one obtained at *R*= 2000 rpm, *d*= 2.0 mm, *T*= 2 s (Figure 9b) has a higher peak temperature (504°C vs 492 °C), which facilitates more eutectic structures in the weld. Although this always deteriorates the mechanical

properties of dissimilar joints, there is no evidence in this case that the joint's failure resulted from the eutectics. On the other side, as in FSW, higher thermal exposure conditions may lead to tunnel defects in the similar welds [18, 19], as a result of excessive flow of plasticized metal off the weld. This might be the case here–the more liquid eutectics were formed, the more material would be lost or off the weld due to filling into the gap between the sleeve and the pin. Moreover, a sufficient extent of liquid eutectics can compromise the shear stress imposed by the tool, which decreases the flowability of the material in solid state, especially when materials of different yield stresses are involved and a turbulent flow behavior occurs. Nevertheless, these are in line with Arbegast's metalworking model [20], where the insufficient forming pressure under the tool prevents the material from consolidating and results in tunnel defects.

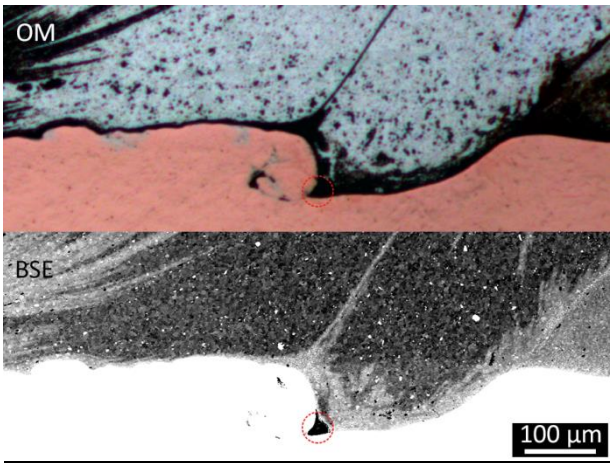


Figure 10. The tunnel defect (indicated by the red circles) at the Al/Cu interface revealed by OM and SEM, whose location indicated by a yellow rectangle on Figure 9b

Table 5. The measured peak temperature for different experiment settings

| *R* (rpm) | *D* (mm) | *T* (s) | Average peak Temperature (°C) |
|---|---|---|---|
| 1200 | 1.6 | 0 | 460 |
| 1200 | 1.8 | 2 | 481 |
| 1200 | 2 | 2 | 478 |
| 2000 | 1.8 | 2 | - |
| 2000 | 2 | 2 | 504 |
| 2000 | 2 | 1 | 492 |

## Conclusions

(1) The results of full-factorial design and ANOVA show that the interaction between the rotational speed and plunge depth significantly influences the LSS at the confidence level of 95%, in addition to the plunge depth. The optimal setting for maximizing the LSS is determined as the rotational speed of 1200 rpm, the plunge depth of 2 mm, and the dwell time of 2 s.

(2) Although all joints failed along the Al/Cu interface, there are two different fracture modes, dependent on the fracture energy resulting from the interlocking effect. In comparison with the load-displacement curves, from a certain stage, the load-bearing structures in both modes have the same component, *i.e.*, a $CuAl_2$-$Al_4Cu_9$ composite layer.

(3) An increase in the plunge depth does not evidently alter the intermetallic composite layer as well as its thickness, but the formed cave on the Al/Cu interface resulting from a large plunge depth behaves as an interlock and thus restrains the crack propagation and changes the fracture mode.

(4) The improved joint LSS due to mechanical interlocking at large plunge depths may be compromised at a high rotational speed because of the formed tunnel defects on the Al/Cu interface.

**References**


[1] K. Savolainen, J. Mononen, T. Saukkonen, H. Hanninen, in: 6th International Friction Stir Welding Symposium, Saint-Sauveur, Canada, 2006, CD-ROM.
[2] J.P. Bergmann, F. Petzoldt, R. Schuerer, S. Schneider, Welding in the World, 57 (2013) 541-550.
[3] M. Marya, S. Marya, Science and Technology of Welding and Joining, 9 (2004) 541-547.
[4] H.J. Liu, J.J. Shen, L. Zhou, Y.Q. Zhao, C. Liu, L.Y. Kuang, Science and Technology of Welding and Joining, 16 (2011) 92-98.
[5] C. Schilling C, J.F. dos Santos, Method and Device for Linking at Least Two Adjoining Work Pieces by Friction Welding. European Patent EP 1230062 B1 (WO 2001/036144), 2004.
[6] T. Rosendo, B. Parra, M.A.D. Tier, A.A.M. da Silva, J.F. dos Santos, T.R. Strohaecker, N.G. Alcantara, Materials & Design, 32 (2011) 1094-1100.
[7] Y.Q. Zhao, H.J. Liu, Z. Lin, S.X. Chen, J.C. Hou, Science and Technology of Welding and Joining, 19 (2014) 617-22.
[8] U.F.H. Suhuddin, V. Fischer, J.F. dos Santos, Scripta Materialia, 68 (2013) 87-90.
[9] U. Suhuddin, V. Fischer, F. Kroeff, J.F. dos Santos, Materials Science and Engineering A, 590 (2014) 384-389.
[10] J. Shen, U. F.H. Suhuddin, M.E.B. Cardillo, J.F. dos Santos, Applied Physics Letters, 104 (2014) 191901 -191904.
[11] J. Shen, M.E.B. Cardillo, J.F. dos Santos, in: 10th International Friction Stir Welding Symposium, Beijing, P.R. China, 2014, CD-ROM.
[12] J. Antony. Design of experiments for engineers and scientists, 2nd ed. Waltham, MA 02451, USA: Elsevier Ltd, 2014.
[13] R.K. Roy. A primer on the Taguchi method, 2nd ed. Dearborn, Michigan 48121: Society of Manufacturing Engineers, 2010.
[14] Minitab 17 Statistical Software. State College, PA: Minitab Inc, 2010.
[15] Specification for Resistance Welding for Aerospace Applications, AWS D17.2/D17.2M: 2013, American Welding Society, 2012.
[16] P.Xue, B.L. Xiao, D.R. Ni, Z.Y. Ma. Enhanced mechanical properties of friction stir welded dissimilar Al-Cu joint by intermetallic compounds. Materials Science and Engineering A. 2010, 527:5723-5727.
[17] C. Genevois, M. Girard, B. Huneau, X. Sauvage, G. Racineux. Interfacial Reaction during Friction Stir Welding of Al and Cu. Metallurgical and Materials Transactions A. 2011, 42:2290-2295.
[18] R.D. Fu, R.C. Sun, F.C. Zhang, H.J. Liu. Improvement of Formation Quality for Friction Stir Welded Joints. Welding Journal. 2012, 91:169s-173s.
[19] P. Periyasamy, B. Mohan, V. Balasubramanian. Effect of Heat Input on Mechanical and Metallurgical Properties of Friction Stir Welded AA6061-10% SiCp MMCs. Journal of Materials Engineering and Performance. 2012, 21:2417-2428.
[20] W.J. Arbegast. Modeling friction stir joining as a metalworking process. Proceedings of Hot Deformation of Aluminum Alloys III. 2003, 313-327.